Corrosion Behavior of Anodized 7B50 Aluminum Alloy in Different Atmospheric Environments

Qiyue Zhao[1], Jinbin Zhao[2], Chuang Guo[1], Haiyan Wang[1], Yunhua Huang[1,], Xuequn Cheng[1], Xiaogang Li[1]*

[1] Corrosion and Protection Center, University of Science and Technology Beijing, Beijing 100083, China
[2] Jiangsu Key Laboratory for Premium Steel Material, Technology Center of Nanjing Iron & Steel Co., LTD, Nanjing 211500, China
[*]E-mail: huangyh@mater.ustb.edu.cn

The corrosion behavior and mechanism of 7B50 aluminum alloy anodized in sulfuric acid solution were studied through outdoor exposure tests in industry-marine and northern semirural atmospheric environments in Qingdao and Beijing, respectively, by means of morphological observation, weight-loss measurement, X-ray diffraction and electrochemical impendence spectroscopy (EIS). The results showed that the average corrosion rates of the anodized alloy decreased by 91.9% and 56.2% after one-year exposure in the industry-marine and northern semirural atmospheric environments, respectively, compared to the naked alloy. Thus the anodic treatment weakened corrosion and the effect was much better in the harsh environment. The high concentration of chloride ions in Qingdao played an important role in the destruction of the oxide films and in inducing the pitting corrosion. Due to the pitting on the grain boundaries and the microgalvanic corrosion among the grain boundary precipitates, precipitate-free zone and the matrix, the intergranular corrosion initiated and propagated throughout the sample. The sulfide in both atmospheres had a remarkable impact on the corrosion of 7B50 Al alloy, which aggravating surface and intergranular corrosion. The aggravation in Qingdao was much more serious. After exposure in Qingdao and Beijing, the anodized film remained an effective hindrance for aggressive ions penetrating to the matrix, and the barrier ability of the alloy in Beijing was better due to the intact double-layer structure of the film as well as the atmosphere's low humidity and low chloride ion concentration. The rust layer formed on the naked alloy was loose and cracked, which could not effectively obstruct the matrix corrosion.

1. INTRODUCTION

7B50 aluminum (Al) alloy belongs to the Al-Zn-Cu-Mg series Al alloy. It is a fourth generation high performance Al alloy developed on the basis of 7050 Al alloy [1]. 7B50 Al alloy has the advantages of high specific strength, low density, high toughness and corrosion resistance, and it has been applied extensively to the main frame, beam, wing siding and other main bearing structural parts of the aircraft [2]. Due to the wide service area of aircraft, the corrosive environment is complex, especially in the industrial-marine atmospheres with industrial pollution, high Cl^- concentration and high humidity characteristics [3]. The corrosion resistance of 7B50 Al alloys is particularly crucial for the life and safety of aircraft.

In recent years, anodizing was the most widely used surface technology for improving the corrosion resistance of Al alloys. The anodized film formed in sulfuric acid has high porosity, good adsorption, thick film layers, good wear resistance and high corrosion resistance [4-5]. In addition, anodizing is widely used for its simple electrolyte composition, convenient operation and low production cost [6-7]. At present, the anodizing process [8-10], the sealing process [11-12], the structural composition of the oxide film [13] and the corrosion behavior of anodized alloys in the salt spray environments [14-16] have been deeply studied. While the published works are mostly concerned with the corrosion resistance, studies focused on corrosion behavior and the mechanism of the anodized Al alloys in long-term exposure are rather scarce.

In this work, the corrosion behavior of a naked and anodized 7B50 Al alloy exposed to the Qingdao industry-marine environment and the Beijing northern semirural atmospheric environment for 1 year was investigated. The corrosion rate was determined by the weight loss method. The composition and the protectiveness of the anodized film and the corrosion products were characterized with microscopic analysis and EIS. The protective nature of the anodized film and the corrosion mechanism of the 7B50 Al alloy were also addressed, which is important to the improvement of the material's environmental adaptability and to ensuring the flight safety of the aircraft.

2. EXPERIMENTAL

2.1 Material Preparation

The specimens used in this study were 7B50 Al alloy. The chemical composition of this alloy is listed in Table 1. The microstructure and the precipitates of the 7B50 Al alloy were investigated by transmission electron microscopy (TEM; FEI TECNAI G20). The TEM specimens were prepared by slicing, grinding and ion thinning.

Table 1 Chemical composition of 7B50 Al alloy

Mg	Si	Zn	Cu	Fe	Mn	Zr	Al
2.12	0.024	6.55	2.07	0.071	0.011	0.14	Bal

The anodized samples of 7B50 Al alloy were obtained with a direct current power supply. The anodizing current density was 2 A/dm^2, and the anodizing time was 30 min. The composition of the electrolyte was 20% sulfuric acid and 20 g/L Al sulfate. The electrolyte solution was maintained at approximately 20°C. After the anodizing process, samples were removed from the electrolytic cell immediately and cleaned with warm distilled water and then sealed in 100°C hot water for approximately 30 min.

2.2 Field Exposure Test

The naked 7B50 Al alloy and anodized 7B50 Al alloy specimens with dimensions of 100 mm×50 mm×3 mm were used for the field exposure test. Before the test, the naked specimens were sequentially ground with 800 grit SiC abrasive papers and then degreased by acetone and ethanol. After all the specimens were weighed (w_0), and their surface areas (S) were measured, the specimens were installed on the atmospheric corrosion exposure supporter at an angle of 45° relative to the ground of the Qingdao (36.05°N, 120.29°E) industry-marine environment and the Beijing (39.98°N, 116.26°E) northern semirural atmospheric environment according to the GB 11112-89 Non-ferrous metals atmospheric corrosion testing method. The exposure duration was 1 year. Four replicated samples were retrieved after six months and 1 year. Three replicas were used to determine the weight loss and the corrosion rate, and the other one was used to analyze the corrosion morphology, corrosion products and electrochemical corrosion behavior. Table 2 lists the environmental parameters and atmospheric pollutants measured at the Qingdao and Beijing experiment stations during the exposure time.

Table 2 Experimental conditions of Qingdao and Beijing experiment stations

Experiment stations	Climate	Weather Factors (annual average)	Corrosion concentration (mg/100cm^2.day)
Qingdao 36.05°N, 120.29°E Altitude：12m	North temperate monsoon climate and ocean climate	Temperature: 12.7 °C Rainfall: 955.2mm Relative Humidity: 74.6%	H$_2$S：0.0607 Sea-salt particles：0.5606 Sulfation rate：0.3287
Beijing 39.98°N, 116.26°E Altitude：73m	Warm temperate and semi - humid, semi-rural atmospheric	Temperature:13.8°C Rainfall: 388.8mm Relative Humidity: 44.6%	H$_2$S：0.0575 Sea-salt particles：0.0313 Sulfation rate：0.2869

2.3 Weight Loss Measurement

After 1 year of exposure, the corrosion products of the specimens were chemically removed by pickling in the solution (20g/L CrO$_3$+50ml/L H$_3$PO$_4$) for 10min at 80°C according to HB5257-83. The specimens were then rinsed with distilled water and dried in air. Then, the samples were weighed to obtain the final weights (w_1). The average corrosion rate after exposure was calculated as follows:

$$V = \frac{W_0 - W_1}{St}$$

where V was the corrosion rate (g·m^{-2}·a^{-1}), w_0 was the original weight (g), w_1 was the final weight (g), S was the surface area (m^2) and t was the exposure time (year).

Corrosion morphologies of the exposed samples with and without anodized film and the corrosion products were observed by scanning electron microscopy (SEM, Quanta 250). The elemental composition of the corrosion products formed on the surface was analyzed using EDS. Furthermore, phase identification was determined by X-ray diffraction (XRD, Rigaku DMAX-RB 12KW).

2.4 Electrochemical Impendence Spectroscopy (EIS) Measurement

After 1 year of exposure, EIS measurements were performed by the Versa STAT 3F electrochemical workstation in 0.1 M NaCl solution using a three-electrode electrochemical cell system, where the specimens were used as working electrode (WE), a platinum plate as counter electrode (CE) and a saturated calomel electrode (SCE) as reference electrode (RE). The electrochemical impedance spectroscopy (EIS) was applied using a potential amplitude of 10 mV on the OCP. The frequency range of 0.01-100000 Hz was used for the EIS experiments. The experimental data were analyzed by software ZsimpWin software.

3. RESULTS AND DISCUSSION
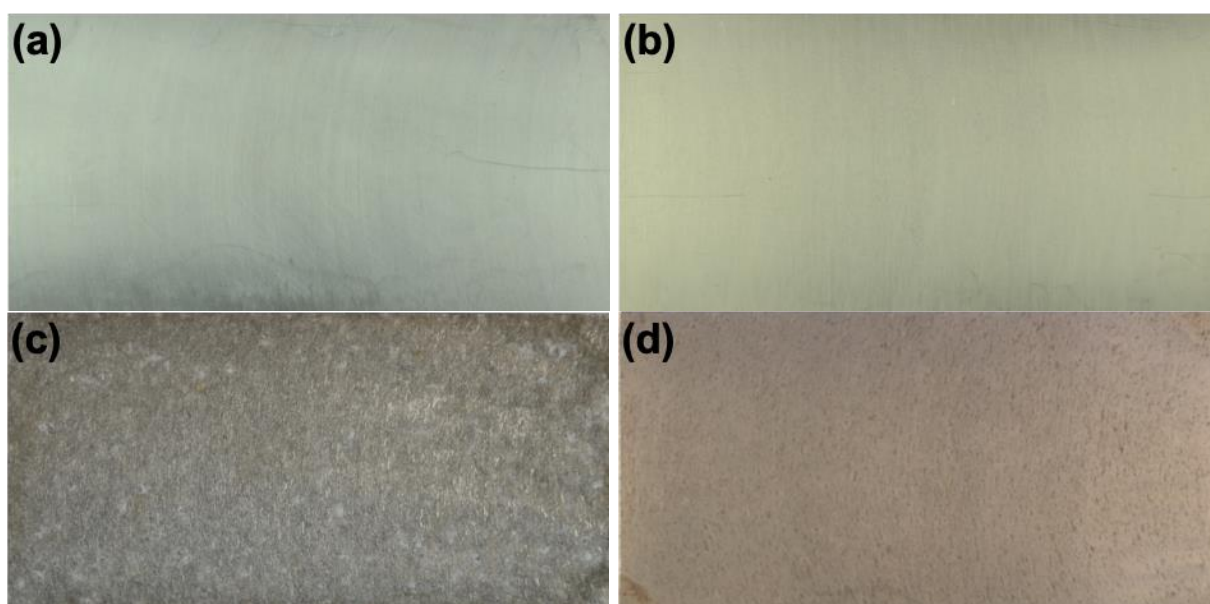
3.1 Weight Loss and Corrosion Rate

The corrosion rates of naked and anodized 7B50 Al alloy after exposure in Qingdao's and Beijing's atmospheres are shown in Table 3. The average corrosion rate of samples in the Qingdao station was greater than that of Beijing, indicating that the 7B50 Al alloy was more susceptible to corrosion in an industrial-marine atmosphere. The humidity of the industrial-marine atmosphere in Qingdao was much higher than that of the northern semirural atmospheric environment in Beijing, where the electrolyte film on the surface of the sample existed for a long time and there were greater concentrations of Cl$^-$ and SO$_2$ in the atmosphere, which accelerated the corrosion rate and corrosion degree of the Qingdao sample. When the naked metal samples with different exposure time were compared, the average corrosion rate of the samples exposed for one year in Qingdao and Beijing for one year was 93.6% and 55.2% of the semiannual samples, respectively, indicating that the corrosion rate of the samples will gradually decrease with time, which might occur because the accumulation of corrosion products and dust and the formation of a new oxide film hindered the further propagation of corrosion. The corrosion rate was gradually controlled by the diffusion rate of the aggressive ions. The weather in Beijing had promoted the accumulation of the dust on the surface of the sample to a certain extent, which has significantly reduced the corrosion rate in one year [17]. For the anodized samples, it was found that the average corrosion rates from Qingdao and Beijing were 8.9% and 43.8% of the naked Al alloys in one year, respectively, which indicated that the anodized film had protected the matrix, and the protection effect is more obvious under the harsh corrosive environment.

Table 3. The average corrosion rate of the samples

City	Sample	Average corrosion rate $g \cdot m^{-2} \cdot a^{-1}$
Qingdao	Naked samples exposed six months	28.52
	Naked samples exposed a year	26.69
	Anodized samples exposed a year	2.35
Beijing	Naked samples exposed six months	5.38
	Naked samples exposed a year	2.97
	Anodized samples exposed a year	1.30

3.2 Surface Morphologies and Corrosion Product Analysis

The macroscopic morphology of the Al alloy specimens after atmospheric exposure is shown in Figure 1. It was clear that the naked sample exposed in Qingdao was heavily corroded, had completely lost its metallic luster and was covered by brown and white corrosion products. The surface of the naked sample exposed in Beijing was not completely covered by the rust layer, and the metallic luster was still visible in some areas. The corrosion products on the surface were punctiform and filamentous. For the anodized samples, the surface processing trace was still distinct, and only point-like corrosion products were formed in some places, which was characterized by local corrosion. Overall, the macroscopic corrosion morphologies of the Qingdao samples' surfaces were more severe than those of Beijing.
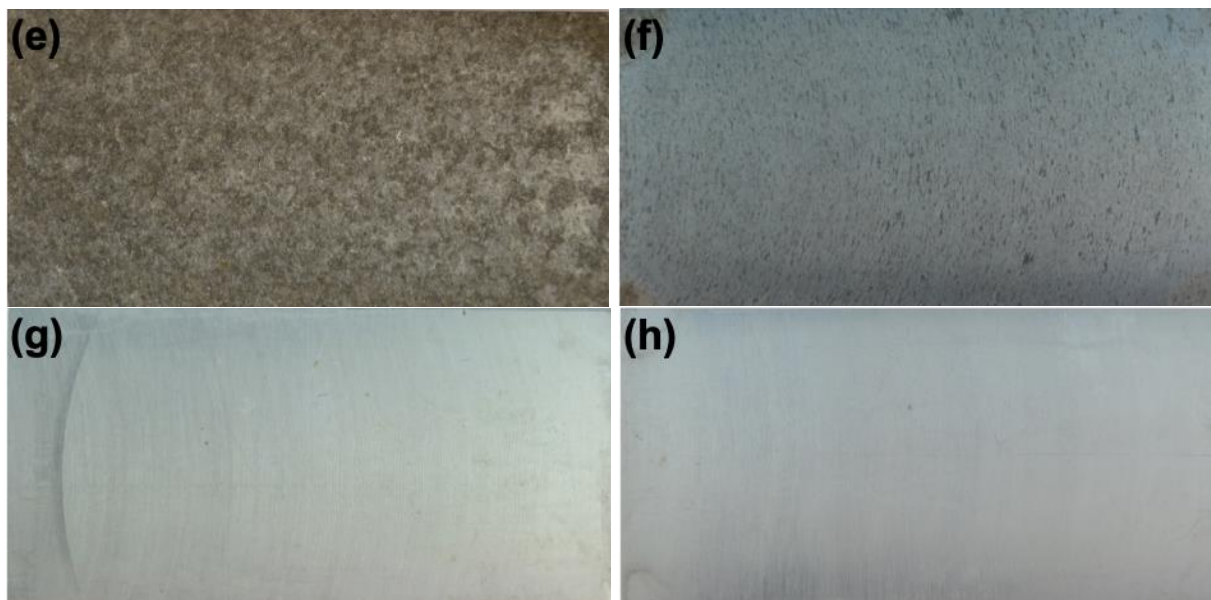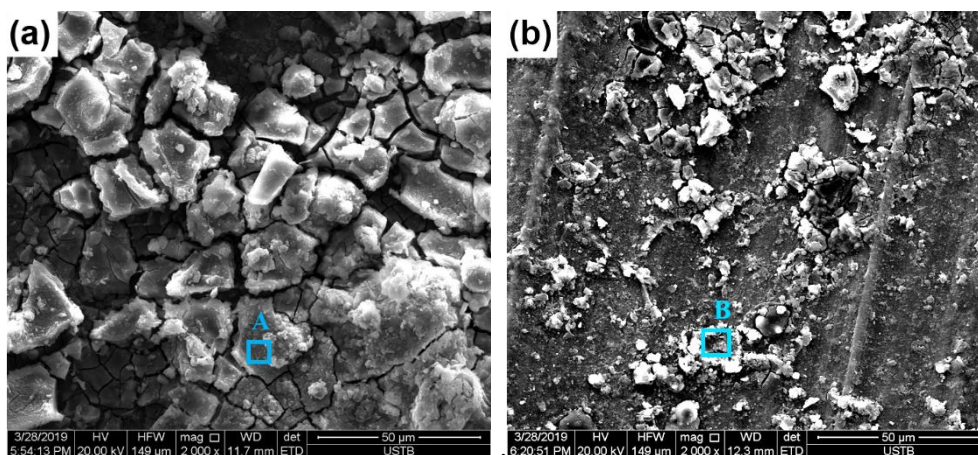
Figure 1. Macro corrosion morphology of each sample before removing the rust (a) initial naked sample (b) initial anodized sample; (c) and (d) Naked samples exposed six months in Qingdao and Beijing; (e) and (f) Naked samples exposed a year in Qingdao and Beijing; (g) and (h) anodized samples exposed a year in Qingdao and Beijing

The microscopic morphologies of the corrosion products on the surface of the exposed samples are shown in Figure 2, and the elemental analysis of the rust layer is shown in Table 4. The surface of the naked sample in Qingdao has been completely covered by cracked corrosion products. In some areas, large amounts of corrosion products appeared. The corrosion products were irregularly stacked on the surface of the Al alloy. While the naked sample exposed in Beijing was also covered with crack-like corrosion products in local areas, but the corrosion products were less and the rust layer was thinner than that of the Qingdao sample. Although there were many cracks on the surface of the Qingdao anodized sample, the whole surface was relatively flat, and only part of the oxide layer was detached due to the pitting corrosion. Moreover, there was only a small number of pits visible on the surface of the anodized sample in Beijing, and no corrosion products accumulated, which is evidence that the corrosion was very slight in Beijing.
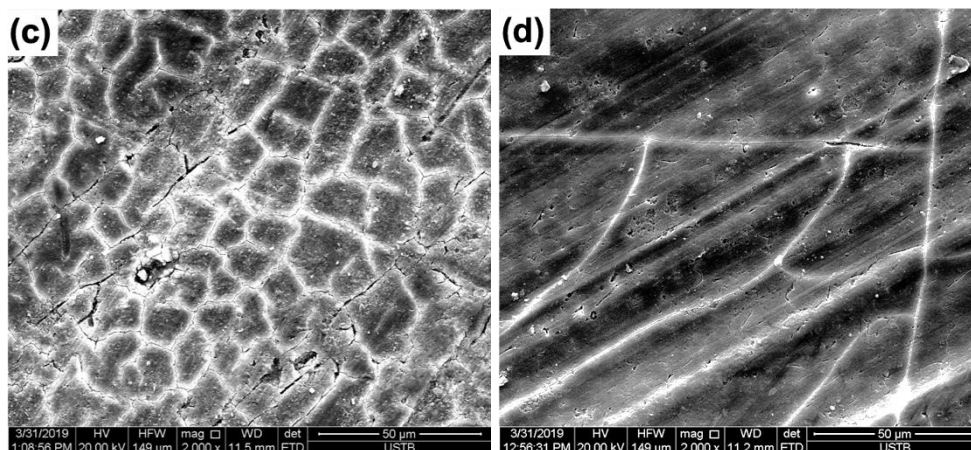
Figure 2. Micro corrosion morphology of each sample after removing the rust. (a) and (b) Naked samples exposed for 1 year in Qingdao and Beijing; (c) and (d) anodized samples exposed for 1 year in Qingdao and Beijing

Table 4. Composition of the rust layer after exposure in Qingdao and Beijing for 1 year

	Al	O	Mg	Zn	Cl	S	Si	Na
A	30.61	41.38	0.82	0.44	6.58	11.51	8.58	2.08
B	39.27	46.40	0.75	0.36	1.95	5.28	4.80	1.19

From Table 4, the contents of S, Cl, Si and Na in the rust layer of Qingdao sample are seen to be significantly higher than those of the Beijing samples, which can be explained by the high levels of salt and pollutants in Qingdao's industrial-marine atmosphere. The naked sample without surface treatment naturally formed a thin oxide film on the surface, while a thick oxide film was artificially formed on the anodized sample. With increased exposure time, the surface of the sample was gradually covered with a layer of dust. In the high salinity and humidity environment in the Qingdao coastal area, Cl$^-$ penetrated the loose soil layer and reached the surface of the sample via the thin electrolyte film, and the pitting corrosion initiated due to the small atomic radius of chloride ion and the quicker migration speed in solution [18]. The autocatalytic action of acid in the pits and the penetration of the corrosive medium caused the corrosion inside the pits to propagate. The pits gradually grew to connect, and a large amount of corrosion products was generated. The accumulation of the corrosion products and dust gradually resulted in stress cracking, and the corrosion products easily fell off under the action of the sea breeze. The specimens that were free of dust and corrosion products were then re-exposed to the atmosphere, which led to deeper levels of corrosion. Since the oxide film was thicker in the anodized sample, the chloride ions had difficulty penetrating the barrier layer to reach the matrix, and the matrix was well protected.

Because of the low chloride ion content and precipitation in the environment in Beijing, the damage to the surface oxide films on both the naked and the anodized samples was relatively mild, which indicated that the protectiveness of the oxide films was still better.
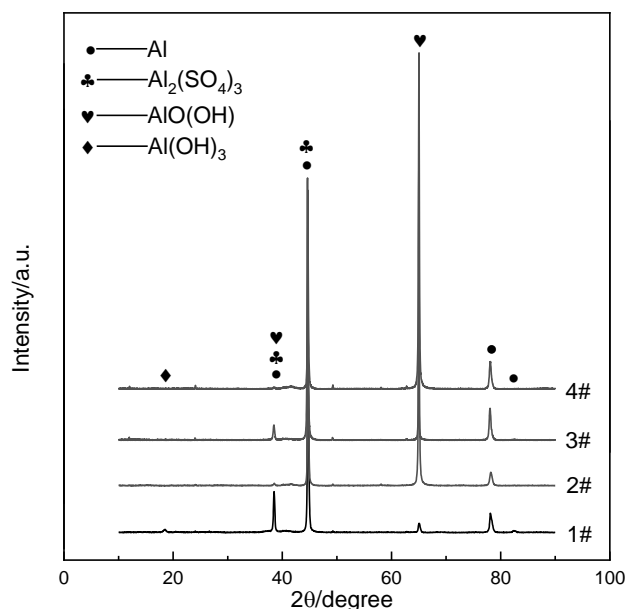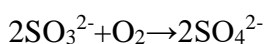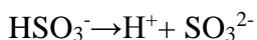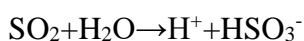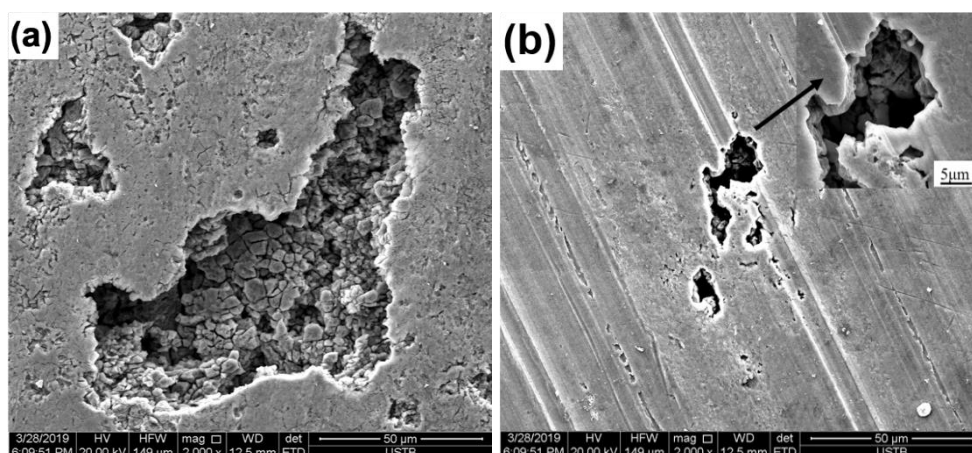
Figure 3. XRD patterns of the samples after exposure (1#) naked and (2#) anodized in Qingdao, and (3#) naked and (4#) anodized in Beijing

The corrosion products of each sample were collected for XRD analysis as shown in Figure 4. The corrosion products were mainly composed of $Al_2(SO_4)_3$, $AlO(OH)$ and trace amounts of $Al(OH)_3$, which indicated that there was no difference in the types of corrosion products in the atmospheric environments of Qingdao and Beijing, but the contents of the products varied. Due to the large amount of SO_2 in the industrial atmosphere of Qingdao, SO_2 could be directly oxidized in the atmosphere to form acid rain. It can also be dissolved into the thin electrolyte film to produce a series of reactions that form SO_4^{2-} and H^+, which increased the conductivity and acidity of the thin electrolyte film and aggravated the corrosion. The reaction process was as follows [19-20]:

$SO_2 + H_2O \rightarrow H^+ + HSO_3^-$

$HSO_3^- \rightarrow H^+ + SO_3^{2-}$

$2SO_3^{2-} + O_2 \rightarrow 2SO_4^{2-}$

$6H^+ + 3SO_4^{2-} + 2Al(OH)_3 \rightarrow Al_2(SO_4)_3 + 6H_2O$

In Beijing, the atmospheric climate was dry with less precipitation, so the corrosion products mainly consisted of $AlO(OH)$ and the amount of $Al_2(SO_4)_3$ was less.
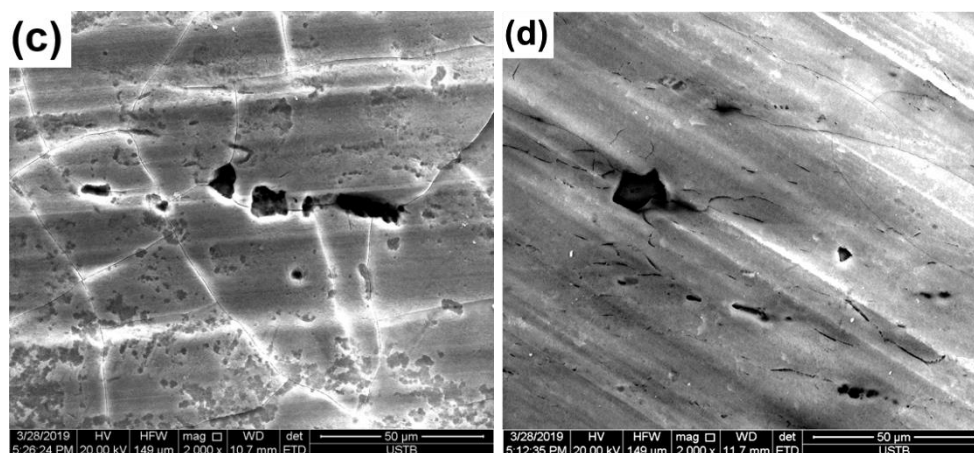
Figure 4. Microscopic morphology of samples after removal of the rust layer (a) and (b) Naked samples exposed for 1 year in Qingdao and Beijing Naked samples Initial sample; (c) and (d) Anodized samples exposed for 1 year in Qingdao and Beijing

The surface morphologies of the rust removal samples are shown in Figure 4. The pits on the surfaces of the naked metal samples in Qingdao and Beijing were irregularly propagated, and the internal layers of the pits were well-defined and deeper. The areas of the pits in Beijing samples were small and the depths were shallow, while the areas of the pits in the Qingdao samples were larger and had obvious intergranular cracks inside. In addition, on the surface of the Qingdao samples, there were many small pits around the large pit, and the pits were inclined to grow. For the sulfuric acid anodized samples, they were obviously less corrosive compared to the naked samples. There were only a few small pits on the surface of the Beijing sulfuric acid anodized sample, and the depth of these pits is shallow. Most of the area was flat, and no obvious corrosion phenomenon could be seen. While there were many pits and cracks evenly distributed on the surface of the Qingdao sample, The difference of the pitting characteristics revealed that the corrosion resistance of the naked and anodized samples were mainly associated with the compactness and the thickness of the film on the surface. In other words, the aggressive ions could not easily to penetrate the anodized film to reach the matrix, thereby reducing the development of the holes [21].
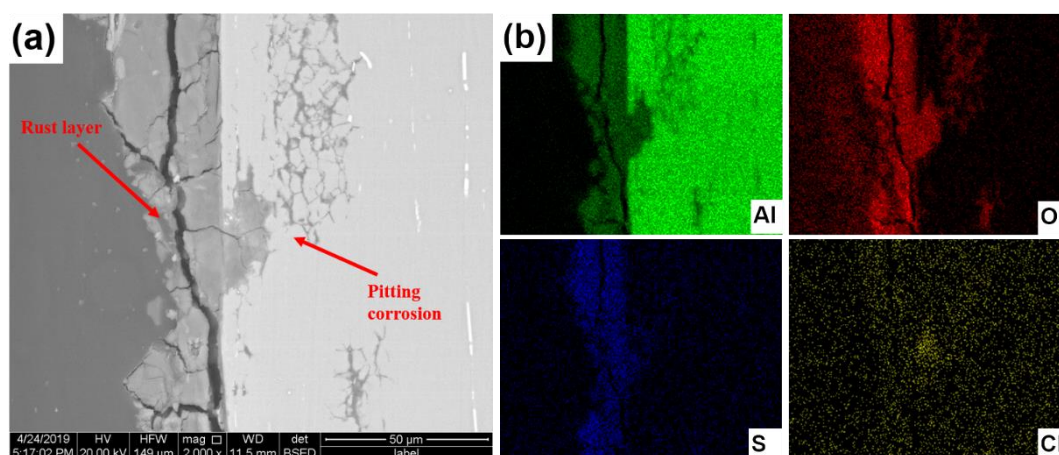
3.3 Cross-sectional Morphology Analysis

Figure 5 shows the cross-sectional morphologies of the corrosion product layer of the naked samples after one-year exposure. As shown in Figure 5(a), (b) and (d), a thick layer of rust appeared on the surface of the Qingdao sample, and the crack in the rust layer was extremely distinct, while the rust layer on the surface of the Beijing sample was thin. The pitting corrosion and the intergranular corrosion (IGC) were observed both in the Qingdao and Beijing samples after one-year exposure. The depth of the pits and the IGC of the Qingdao sample were much larger than those of the Beijing sample. Additionally, the cracks along the grain boundary were filled with loose corrosion products. When a unit cell with severe intergranular corrosion happens to be on the surface of the sample, the entire grain may fall off of the surface of the sample. Then, ablation occurs, which is correspondent with the surface morphology in Figure 2. In the marine atmosphere of Qingdao, the deposition of chloride-containing particles on the

surface of the sample destroyed the oxide film of the 7B50 Al alloy, which induced pitting corrosion. In the case where the pitting occurs on the grain boundaries, IGC initiates [22]. However, in the northern semirural atmospheric environment of Beijing, the oxide film was difficult to be destroyed and the pitting corrosion was not easily initiated and propagated mainly due to the fewer chloride ions and drier climate than that in Qingdao.

In the 7B50 Al alloy, both grain boundary precipitates (GBP) and precipitate-free zone (PFZ) along the grain boundaries were observed as shown in Figure 6 and PFZ was approximately 30-60nm on either side of the boundary, in which Mg, Zn and Cu depletions were expected. The fine precipitates along the grain boundary were composed of Mg, Al, Zn and Cu, which the $MgZn_2$ precipitates with considerable solubility of Cu and Al [23]. The segregation of Mg, Zn and Cu from the matrix has created a depleted zone where the chemical composition is inclined to pure Al, which resulted in the PFZs adjacent to the grain boundaries having different electrochemical properties from the 7B50 Al alloy matrix and the precipitates along the grain boundaries. The open circuit potential of pure Al alloy was much lower than that of the bulk alloy and the intermetallic phases in the Al alloy [24-25], so the depleted regions next to the grain boundaries preceded corrosion, which led to the formation of the IGC pathways. Then, the GBP fell off along the pathways, and the IGC propagated. As the exposure time increased, the thin networks of IGC extended into the matrix, and the corrosion pathways became more distinct [26].

The elemental distribution of surface corrosion products and IGC products are shown in Figure 7 (b)-(e). Both of the corrosion products were found to contain large amounts of Al and O elements, and the content of the O element in the surface corrosion products was slightly higher than that in the IGC products. The Cl element showed no significant aggregation in either the surface corrosion products or IGC products in both the Qingdao and Beijing samples. While the S element was well distributed in the surface products, and the S enrichment could also be observed in the IGC region of Qingdao sample, indicating that the sulfide contaminant in the atmospheric environment had a great influence not only on the surface but also the IGC region. When the sulfide dissolves in the thin electrolyte film to form sulfite ions and penetrates into the grain boundary region, it provided the microgalvanic corrosion of the grain boundary region with a favorable corrosive medium, which aggravated the IGC. The depth of pitting and IGC was mainly attributed to the dry climate in Beijing, and no thin electrolyte film was formed on the surface. This played an essential role in the development of the pitting and IGC.
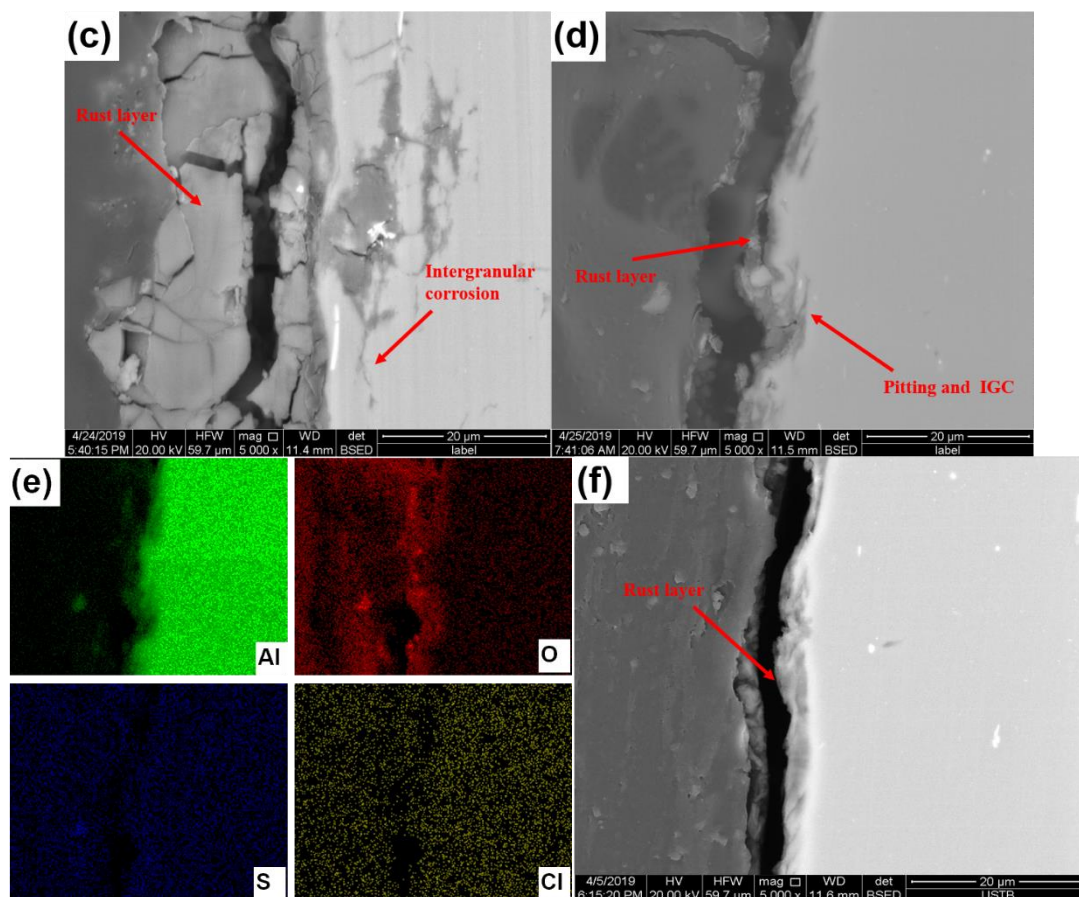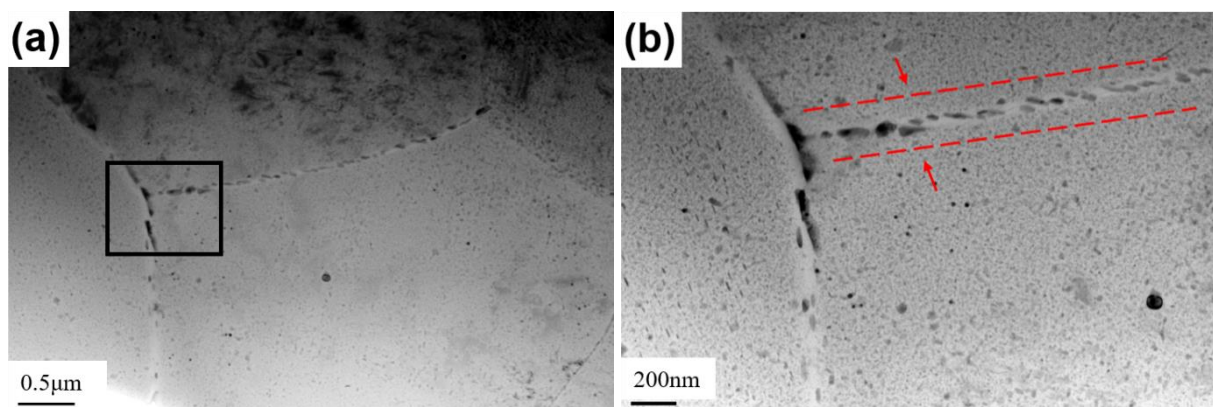
Figure 5. Cross-sectional morphologies of the naked samples of after one-year exposure (a) and (c) in Qingdao; (d) and (f) in Beijing and the distribution of elements of (b) the Qingdao sample and (e) the Beijing sample

Figure 7 shows the cross-sectional morphologies of the corrosion product layer of the anodized samples after one-year exposure and no obvious intergranular cracks have been seen. Figure 7(a) shows the exposed sample from Qingdao. The outer layer of the oxide film has been destroyed and the pitting pit penetrated the oxide film and eroded down the matrix. Figure 7(b) shows the exposed sample from Beijing. The double-layer structure of the anodized film was still relatively intact and no obvious damage could be seen on it, which indicated that the protectiveness of the oxide film of the sample from Beijing after one-year exposure was much higher than for the sample from Qingdao.
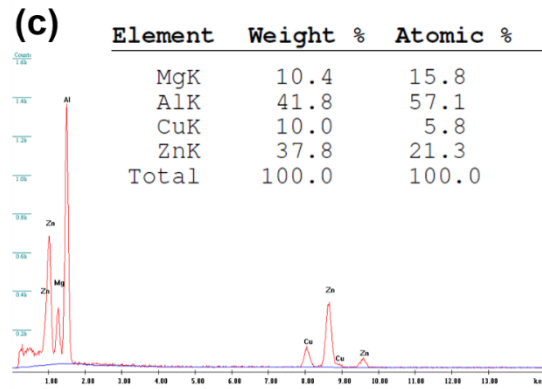
Element	Weight %	Atomic %
MgK	10.4	15.8
AlK	41.8	57.1
CuK	10.0	5.8
ZnK	37.8	21.3
Total	100.0	100.0

Figure 6. TEM images of (a)-(b) the precipitates along the grain boundary and (c) EDS of the precipitates

Element	Wt%	At%
OK	38.80	52.63
MgK	00.67	00.60
AlK	51.56	41.47
SK	05.99	04.06
ClK	00.25	00.15
ZnK	02.27	00.75

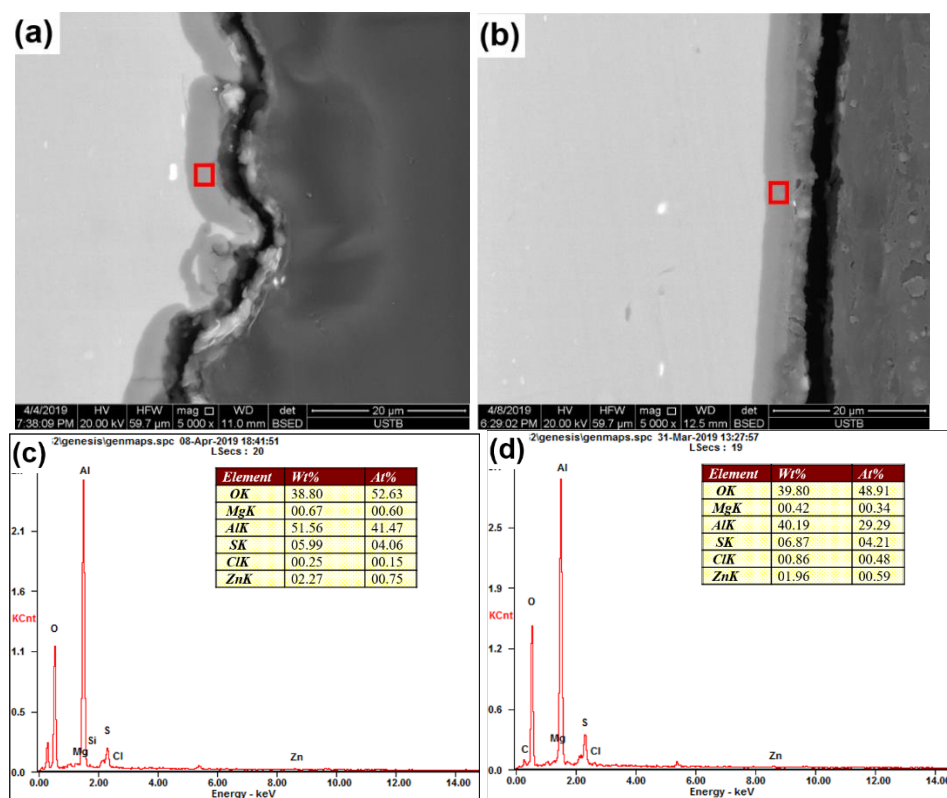| Element	Wt%	At%
OK	39.80	48.91
MgK	00.42	00.34
AlK	40.19	29.29
SK	06.87	04.21
ClK	00.86	00.48
ZnK	01.96	00.59

Figure 7. Cross-sectional morphologies and EDS analysis of the anodized samples of (a) and (c) Qingdao; (b) and (d) Beijing

3.4 EIS Measurements

EIS is an efficient method to study the surface conditions of metals and a good tool to evaluate the protectiveness of the corrosion product layer and oxide film [27-30]. EIS of the 7B50 Al alloy after one-year exposure in Qingdao and Beijing are shown in Figure 8. The impedance spectra of both the naked and the anodized samples exhibited two capacitive loops, and the sizes of the impedance arc radii of the anodized samples were much larger than those of the naked samples. The sizes of the impedance arc radius of the Qingdao exposure samples were smaller than those of Beijing samples.

The equivalent circuit model in Figure 9 is used for fitting the EIS data in Figure 8. In the model, Rs is the solution resistance, Q_f and R_f are the constant phase element of the corrosion product layer or the oxide film, respectively, and Q_{dl} and R_{ct} are the double layer capacitance and the charge transfer resistance, respectively. In the EIS, the polarization resistance (R_p) can be obtained when $\omega \to 0$ which can characterize the difference in the corrosion resistance of the materials. The larger the polarization resistance, the better the corrosion resistance of the materials [31]. In the model shown in Figure 9, R_p can be calculated as follows:

$$R_p = R_f + R_{ct}$$

The R_p of the naked 7B50 Al alloy samples as well as anodized samples are shown in Figure 10. The R_p of the anodized samples exhibited larger values than that of the naked Al alloy. As the double-layer structure of the oxide film of the Beijing anodized sample was still relatively intact, the chloride ions could not easily penetrate the anodized film to reach the matrix. The outer layer of the Qingdao anodized sample was destroyed, and the barrier ability of the oxide film was less than that of the Beijing sample, which resulted in the R_p of the Qingdao sample being much smaller than that of the Beijing sample. For the naked samples from the two stations, there was a significant difference in the corrosion resistance of the rust layer. The rust layer of the Qingdao sample was loose and cracked and the pitting was distributed all over the surface where the aggressive ions could easily penetrate into the matrix. There were less corrosion products on the Beijing naked sample, and the rust layer was more complete than Qingdao sample, which led to a larger R_p and better corrosion resistance. Overall, the protectiveness of the anodized film was far stronger than that of the rust layer even after one-year exposure, which was consistent with the previous weight loss results.
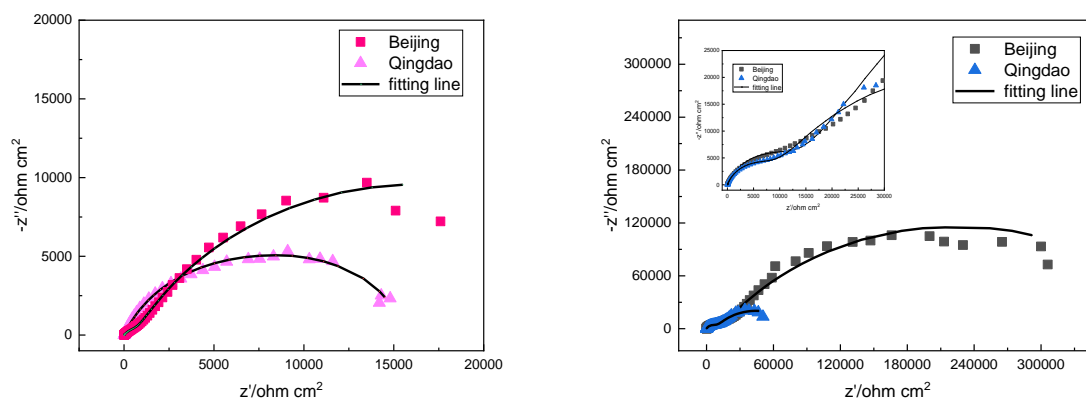

Figure 8 Nyquist diagram of (a) naked 7B50 samples and (b) anodized samples after one-year exposure in Qingdao and Beijing
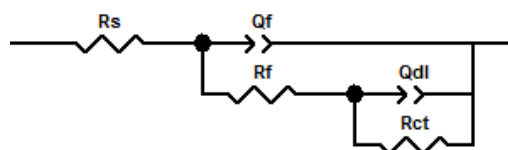

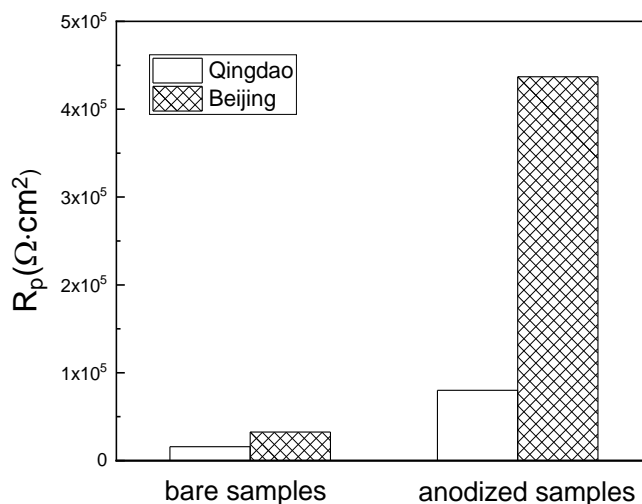**Figure 9.** Equivalent circle of the exposed 7B50 Al alloy

Figure 10. Calculated polarization resistance (R_p) of the exposed 7B50 Al alloy

4. CONCLUSIONS

(1) The field exposure tests showed that anodizing in sulfuric acid can significantly reduce the average corrosion rate of 7B50 Al alloy, and the effect was more efficient in the industrial-marine atmospheric environment than that in the northern semirural atmosphere. Compared with the naked alloy, the average corrosion rates of the anodized alloy in Qingdao and Beijing decreased by 91.1% and 56.2%, respectively.

(2) The high concentration of chloride ions in Qingdao's industrial-marine atmosphere played an important role in destroying the oxide films and inducing the pitting corrosion on both the naked and the anodized alloys. In the case where the pitting occurred on the grain boundaries, IGC initiated and then propagated, which can be attributed to the microgalvanic corrosion among the GBP, PFZ and the matrix.

(3) The sulfide in both atmospheres had a remarkable impact on the corrosion of the 7B50 Al alloy. Sulfide aggravated the surface and intergranular corrosion, the aggravation in Qingdao was much more serious. In Qingdao's atmosphere, the sulfide converted to sulfite ions and penetrated to the matrix and the grain boundary region, which provided a favorable corrosion medium for the pitting and IGC.

(4) The anodized film after exposure in Qingdao and Beijing remained an effective hindrance for aggressive ions penetrating to the matrix after exposure, and the barrier ability of the alloy in Beijing was better due to the intact double-layer structure of the film and the atmosphere's low humidity and low chloride ion concentration. The rust layer formed on the naked alloy was loose and cracked and could not effectively obstruct the matrix corrosion.

References

1. P. Gong, L. Zheng, K. Zhang, L. Yi and D. Song, *J. Aeron. Mater.*, 31 (2011) 45.
2. L. Kang, G. Zhao, N. Tian and H. Zhang, *Trans. Nonferrous Met. Soc. China*, 28 (2018) 989.
3. B. Zaid, D. Saidi, A. Benzaid and S. Hadji, *Corros. Sci.*, 50 (2008) 1841.
4. Y. Zhao, M. Chen, Y. Zhang, T. Xu and W. Liu, *Mater. Lett.*, 59 (2005) 40.
5. Y. Li, Y. Qin, S. Jin, X. Hu, Z. Ling, Q. Liu, J. Liao, C. Chen, Y. Shen and L. Jin, *Electrochem. Acta*, 178 (2015) 11.
6. J. Ren and Y. Zuo, *Appl. Surf. Sci.*, 261(2012) 193.
7. E. Zalnezhad, A. Sarhan and M. Hamdi, *Int. J. Adv. Manuf. Tech.*, 68 (2013) 453.
8. J. Liu, Y. Li, M. Yu, S. Li and Y. Sun, *Chin. J. Nonferrous Met.*, 22 (2012) 324.
9. S. Wang, Q. Zhao, N. Du, Z. Shao, W. Shu and Q. Chen, *Chin. J. Nonferrous Met.*, 22 (2012) 1132.
10. S. Li, W. Yao, J. Liu, M. Yu, L. Wu and K. Ma, *Surf. Coat. Technol.*, 277 (2015) 234.
11. G. Yoganandan, J. Balaraju, C. Low, G. Qi and Z. Chen, *Appl. Surf. Sci.*, 288 (2016) 115.
12. D. Zhang, G. Dong, Y. Chen and Q. Zeng, *Appl. Surf. Sci.*, 290 (2014) 466.
13. D. Kong, J. Wang and H. Liu, *Chin. J. Nonferrous Met.*, 24 (2014) 174.
14. R. Zhou, X. Li and C. Dong, *Eq. Environ. Eng.*, 3 (2006) 1.
15. C. Feng, Y. Huang, Y. Shen, K. Xiao, F. Meng and X. Li, *Eq. Environ. Eng.*, 12 (2015) 100.
16. D. Kong and J. Wang, *J. Alloys Compd.*, 632 (2015) 286.
17. B. Wang, Z. Wang, W. Han and W. Ke, *Corros. Sci.*, 59 (2012) 63.
18. S. Wang, L. Yang, K. Xiao, Y. Huang and X. Li, *Chin. J. Eng.*, 40 (2018) 833.
19. Y. Xiang, Z. Wang, C. Xu, C. Zhou, Z. Li and W. Ni, *J. Supercrit. Fluids.*, 58 (2011) 286.
20. A. Elola, T. Otero and A. Porro, *Cororsion*, 48 (1992) 854.
21. M. Mubarok, Wahab and Sutarno, *J. Miner. Mater. Charact. Eng.*, 3 (2015) 154.
22. Z. Cui, X. Li, C. Man, K. Xiao, C. Dong, X. Wang and Z. Liu, *J. Mater. Eng. Perform.*, 24 (2015) 2885.
23. T. Ramgopal, P. Gouma and G. Frankel, *Corrosion*, 58 (2002) 687.
24. T. Burleigh, E. Ludwiczak and R. Petri, *Corrosion*, 51 (1995) 50.
25. L. Huang, K. Chen, S. Li and M. Song, *Scr. Mater.*, 56 (2007) 305.
26. H. Li, Q. Mao, Z. Wang, F. Miao, B. Fang, R. *Mater. Sci. Eng. A*, 617 (2014) 165.
27. J. Wang, Z. Wang and W. Ke, *Mater. Chem, Phys.*, 139 (2013) 225.
28. H. Katayama and S. Kuroda, *Corros. Sci.*, 76 (2013) 35.
29. Z. Cui, X. Li, K. Xiao and C. Dong, *Corros. Sci.*, 76 (2013) 243.
30. L. Kong, K. Wang, Y. Zhan, and Y. Zhang, *Int. J. Electrochem. Sci.*, 12 (2017) 2982.
31. T. Zhang, Y. Shao, G. Meng, Z. Cui and F. Wang, *Corros. Sci.*, 53 (2011) 1960.